ELSEVIER

Journal of Magnetism and Magnetic Materials 225 (2001) 17–20

Journal of magnetism and magnetic materials

www.elsevier.com/locate/jmmm

Iron nanoparticles as potential magnetic carriers

Everett E. Carpenter*

Complex Materials Section 6342, Naval Research Laboratory, 4555 Overlook Avenue SW, Washington, DC 20375, USA

Abstract

Using a sequential synthesis offered by reverse micelles, stable magnetic nanoparticles based on iron can be formed. Sequential synthesis allows an iron core to be passivated by a thin layer of gold. These nanocomposite materials offer enhanced magnetic properties over existing iron oxide-based particles as well as reduced non-specific binding of proteins due to the small size. Published by Elsevier Science B.V.

Keywords: Nanoparticle synthesis; Core-shell; Reverse micelle; Magnetic carriers; Superparamagnetic; Magnetic nanoparticle; Gold-coating; Iron nanoparticle; Micelle; Non-specific binding

1. Introduction

Over the past 10 years the computer and semiconductor industry has been fueling an explosive growth in materials research to reach the lofty goals required by the market. This explosion has pushed research for new materials into the nanometer size regime. Nanoparticles have been synthesized in a variety of methods ranging from sputtering to chemical vapor deposition [1]. Currently, one of the most versatile methods explored are wet chemical methods such as the microemulsion technique [2].

Microemulsion techniques rely on the self-assembly nature of surfactants to push aqueous reactants into a micelle. Due to the dynamic nature of micelles, aqueous components can come together and react to form particles that are constrained to the size of the micelle. By changing the reaction conditions the methods can even be applied sequentially to form core–shell structures [3]. Originally, this sequential methodology was used with similar materials such as CdS/CdSe, and CdS/ZnS [4,5]. The synthesis using reverse micelles offers a preferred method for preparing nanoparticles that have a very narrow size distribution and very uniform morphology. Synthesizing core–shell structures has many advantages, such as tailoring the magnetic properties, functionalizing the particles, and protecting the particles [6]. Iron nanoparticles often are pyrophoric due to their high surface area. By coating an iron nanoparticle with a stable noble metal like gold, the iron is protected from oxidation. Further, since gold is diamagnetic the magnetic properties of iron would not be adversely affected.

2. Experimental

The reverse micelle reaction is carried out using cetyltrimethylammonium bromide (CTAB) as the

* Tel.: +1-202-767-6296; fax: +1-202-404-8849.
E-mail address: carpenter@anvil.nrl.navy.mil (E.E. Carpenter).

0304-8853/01/$ - see front matter Published by Elsevier Science B.V.
PII: S0304-8853(00)01222-1

surfactant, octane as the oil phase, and aqueous reactants as the water phase [7]. Varying the water to surfactant ratio (ω) can form micelles ranging in size from 5 to 30 m thus leading to careful control over the particle size. A co-surfactant of *n*-butanol is used to help decrease the fraction of the micellar head group that is neutralized and thereby increase the stability of the micelle [8]. Without the addition of the co-surfactant, the amount of free water available to carry on the reactions is greatly reduced, as most of the water is locked in the head group of the CTAB [9].

The metal particles are formed inside the reverse micelle by the reduction of a metal salt using sodium borohydride. The sequential synthesis offered by reverse micelles is utilized to first prepare an iron core by the reduction of ferrous sulfate by sodium borohydride. After the reaction has been allowed to go to completion, the micelles within the reaction mixture are expanded to accommodate the shell using a larger micelle containing additional sodium borohydride. The shell is formed using an aqueous hydrogen tetrachloroaurate solution. The particles are then washed, collected in a magnetic field and dried under vacuum. The dried powder is analyzed using powder X-ray diffraction (XRD), SQUID magnetometry, transmission electron microscopy (TEM) and electron dispersive absorption spectroscopy.

3. Results

A typical XRD plot is presented in Fig. 1. The plot reveals a typical pattern for face centered cubic (FCC) gold. The pattern for a body centered (BCC) iron is obscured under the gold. During extended scan times, the overlapping peaks begin to separate, but due to the extended times needed to resolve iron from gold, XRD is used to confirm the presence of gold. This conclusion is also confirmed in the electron diffraction patterns where there is a diffusion of the rings due to a slight mismatch between the overlapping of 200, and 220 of the FCC gold diffusion rings with 110, and 220 of the BCC iron rings. Although diffraction studies cannot differentiate between iron and gold in the system, they do demonstrate a high degree of crystallinity and uniformity in the particles. The peak location can be indexed to that of FCC gold structure [10]. A representative transmission electron micrograph is presented in Fig. 2.

Elemental analysis of the particle was carried out using EDAX attached to a TEM. By focusing the electron beam to two nanometers on EDS mode, the results showed that the particles are 67% iron and 33% gold corresponding to a particle which is 7 nm in diameter coated with a 1 nm thick shell of gold. This was confirmed with the magnetic characterization. A representative magnetic susceptibility

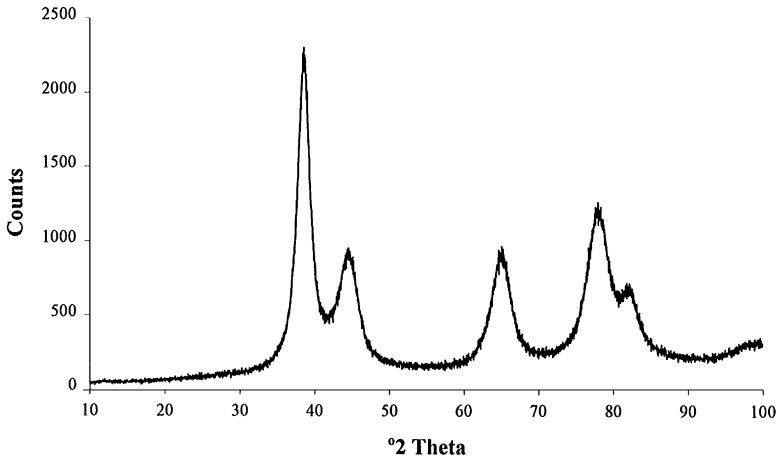

Fig. 1. A typical powder diffraction pattern collected using a Phillips-Norelco X-ray diffractometer with a graphite monochromator and PMT detector. The peaks can be indexed to the reference pattern of gold and iron.

plot, presented in Fig. 3, exhibits a cusp in the zero-field cooled (ZFC) susceptibility at the blocking temperature, T_B. Above T_B, in the superparamagnetic regime, the particles are free to align with the field during the measuring time and depart from the ZFC susceptibility at a temperature near the ZFC maxima and monotonically increase below this temperature. For a superparamagnetic system, the blocking temperature is dependent upon the measuring field.

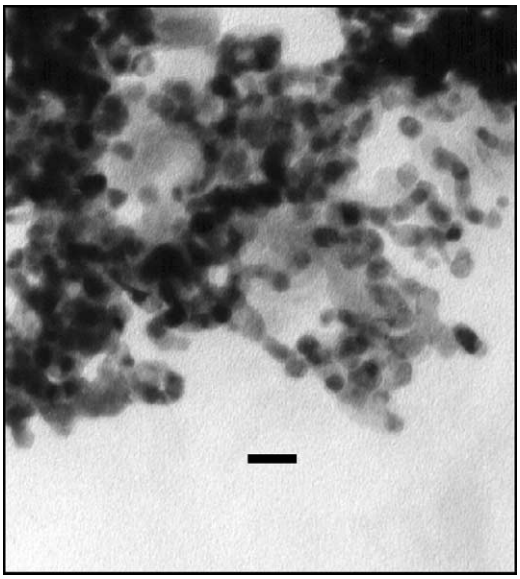

Fig. 2. TEM image of a sample of 12 nm iron–gold particles (dark spots). Lighter areas are the surfactant CTAB. The bar length equals 25 nm.

Below the temperature where the nanocomposites have superparamagnetic behavior, the nanomaterials reveal a remanent magnetization and coercivity. The inset in Fig. 3 records the magnetization of the gold-coated iron, Au@Fe, sample as the magnetic field of the susceptometer cycles between $+50$ and -50 kOe. Remanent magnetization (M_R) and coercivities (H_C) for all nanoparticles are 13.67 emu/g and 400 Oe, respectively. Above the blocking temperature, in the superparamagnetic regime, no coercivity or remanence is observed. An estimate of the average magnetic size can be obtained from the slope of the magnetization near zero field. As stated in Ref. [11], the major contribution to the slope near zero field for superparamagnetic particles with a size distribution, comes from the largest particles and therefore, an upper bound for the magnetic size may be estimated. Using the data shown in Fig. 3 and according to the equation,

$$d_{\max} = \left[\frac{18kT}{\pi} \frac{(\mathrm{d}M/\mathrm{d}H)_{H=0}}{\rho M_s^2} \right]^{1/3},$$

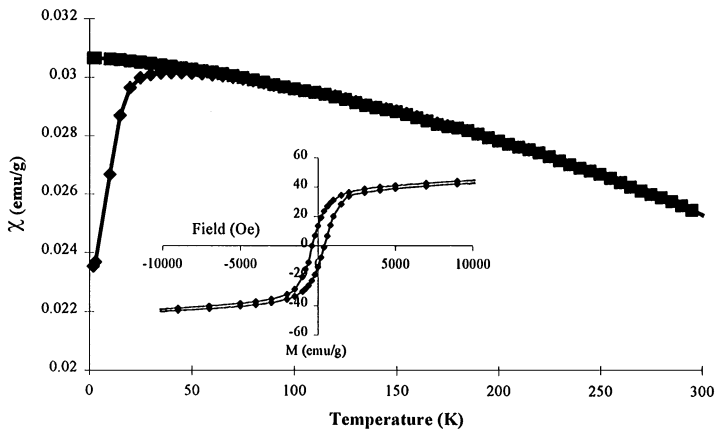

Fig. 3. Field-cooled and zero-field-cooled magnetic susceptibility versus temperature plot. The samples were cooled and measured in an applied field of 1000 Oe. The inset presents a magnetization versus field plot measured at 10 K at a field sweep between -50 and 50 kOe.

where d_{max} is the maximum diameter, k the Boltzmann constant, T the temperature (100 K), dM/dH = the slope near zero field (0.0308 emu/g Oe), and ρ is the density of iron (7.97 g/cm^3), the magnetic particle size for Fe can be determined. Assuming that the saturation magnetization, M_S corresponds to that of the bulk material (220.7 emu/g), the magnetic diameter of the particles is 4.1 nm. This is different from that calculated from the elemental analysis collected from EDAX but not unexpected. It is common with nanoparticles synthesized in reverse micelles to have a layer on the surface that is magnetically 'dead'. This comes from disordered surface spins on the iron core [12]. The thickness varies with the reaction conditions but is usually between 1 and 2 nm thick.

Table 1
For comparison purposes, two commercial magnetic carriers were dried and prepared in a manner similar to the gold–iron nanocomposites

Material	Size diameter (nm)	Iron content (%)	Susceptibility at 300 K (emu/cm^3)
Seramag	850	17	3.29×10^{-6}
Dynal	2400	12	2.72×10^{-6}
Gold–Iron	12	65	6.57×10^{-5}

4. Conclusions

This work demonstrates a method for the synthesis of a uniform nanocomposite made from iron with a gold shell. Since the coating is uniform, the particles are not air-sensitive unlike most metal nanoparticles. This allows for a much smaller and more versatile magnetic nanoparticles with potential uses as a magnetic carrier.

The magnetic properties of the particles are compared with two other commercial magnetic carriers, Seramag M-280 and Dynal Dynabeads in Table 1. In each case, the commercial products rely on magnetic iron oxides. Iron nanoparticles offer an order of magnitude greater susceptibility at room temperature. This translates to lower magnetic fields needed to manipulate the particles or improved localization of the particles. In addition to the improved magnetic properties, gold-coated iron nanoparticles have increased functionality as a result of the very diverse chemistry associated with gold.

The smaller size of the particles allows additional advantages. The particles have a much lower surface area reducing non-specific protein binding. Since many immunological responses rely on surface antigen recognition, the smaller size should result in a reduced immunological response. The smaller size and improved magnetic properties combined suggest that iron-based magnetic carriers would be superior to the existing iron oxide-based carriers.

Acknowledgements

The Advanced Materials Research Institute supported this work through DARPA grant no. MDA972-97-1-0003.

References

[1] J. Weissmuller, Nanomaterials: Synthesis, Properties and Applications, Institute of Physics Publishing, Philadelphia, 1996.
[2] H. Wennerstrom, O. Soderman, U. Olsson, B. Lindman, Colloids Surf. A 123 (1997) 13.
[3] M. Pileni, P. J. Phys. Chem. 97 (1993) 6961.
[4] H.S. Zhou, I. Honma, J.W. Haus et al., Luminescence 70 (1996) 21.
[5] Y. Tian, T. Newton, N.A. Kotov et al., J. Phys. Chem. 100 (1996) 8927.
[6] C.J. O'Connor, E.E. Carpenter, C. Sangregorio, Mol. Crystals Liquid Crystals 335 (1998) 641.
[7] M. Boutonnet, J. Kizling, P. Stenius, Colloids Surf. A 5 (1982) 209.
[8] M. Valiente, E.J. Rodenas, Colloids Inter. Sci. 127 (1989) 522.
[9] M. Valiente, E.J. Rodenas, Am. Chem. Soc. 95 (1991) 3368.
[10] Reference X-Ray Powder Diffraction Patterns, International Centre for Diffraction Data, Newtown Square, PA, 1996.
[11] I.I. Yaacob, A.C. Nunes, A.J. Bose, Colloid Inter. Sci. 171 (1995) 73.
[12] F. Bodker, S. Morup, S. Linderoth, Phys. Rev. Lett. 72 (1994) 282.